Biophysical Chemistry 14 (1982) 205–216
Elsevier/North-Holland Biomedical Press

ELECTRIC AND OPTICAL ANISOTROPY AND THEIR OSMOTICALLY INDUCED CHANGES OF PHOTORECEPTOR DISK MEMBRANE VESICLES

Hideo TAKEZOE † and Hyuk YU *

Department of Chemistry, University of Wisconsin, Madison, WI 53706, U.S.A.

Received 22 August 1980
Revised manuscript received 13 April 1981

Electro-optical characterization of the photoreceptor disk membrane vesicle is performed by examining the electric field and concentration dependence of the steady-state birefringence of aqueous suspensions of the vesicles. The electric polarizability anisotropy is found to be negative and of large magnitude: $\alpha_1 - \alpha_2 = -(1\text{–}3) \times 10^{-10}$ cm^3. The optical anisotropy is determined to be also negative but of small magnitude: $g_1 - g_2 = -1 \times 10^{-7}$. The specific Kerr constant deduced from the concentration dependence of the Kerr constant is found to be very large: $K_{sp} = 7 \times 10^{-4}$ e.s.u. Upon deforming the vesicles osmotically from the spherical shell to the disk structure, the steady-state birefringence increases by an order of magnitude which is attributed solely to the increase in optical anisotropy attending the corresponding change in the geometric eccentricity of the vesicle. A plausible birefringence mechanism based on the known structural features of the vesicles is proposed, which would account for these findings.

1. Introduction

We present here an electro-optical characterization of a novel structure arising from the osmotically swollen vesicles of the photoreceptor disk membranes. Any biological membrane surface is a complex electrostatic entity [1,2] and that of a photoreceptor disk membrane is no exception [3]. Hence, a study of the static Kerr effect provides us with insights into the electrical and optical properties of the membrane surface. To our knowledge, this is the first time that the electro-optical characterization of a well defined biological membrane system has been reported.

The gross characterization of the disk membrane vesicles (DMV) has been effected in the past several years in this laboratory. Upon isolating the disk membranes from the outer segment of rod cells of bovine retina [4], they are swollen into vesicles and dilute suspensions of DMV are made in hypotonic media. By elastic (total intensity) and quasi-elastic light scattering, it has been shown that a DMV is well represented by a spherical shell model with a radius of 450–480 nm and its size distribution is relatively narrow [5]. Because of such a large size of the swollen vesicles, the bilayer thickness of 70–80 Å [6] makes a negligible contribution to the overall dimension whereby the spherical shell model representation is most appropriate. By a deswelling study with the use of an impermeable solute, e.g., sucrose [7], in the suspending medium, it has in turn been shown that the spherical shell deforms into an oblate shell with its semi-major axis dimension unchanged [8]. Other morphological studies corroborate this finding [9], and the conserved semi-major axis plane appears to be the disk plane in the native rod outer segment. Thus, we are dealing with a simple shape of the spherical shell with an equator rim which differs structurally from the upper and lower hemispheres. A summary of these structural features is schematically represented in fig. 1.

Besides such a structural simplicity, the disk membranes are also singular in chemical simplic-

† On leave from Department of Textile and Polymeric Materials, Tokyo Institute of Technology, Tokyo, Japan.

* To whom correspondence should be addressed.

0301-4622/81/0000–0000/$02.50

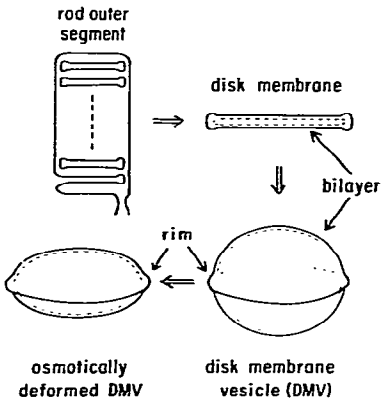

Fig. 1. A schematic representation of a rod outer segment, an isolated disk, a DMV in spherical shell and oblate shell states.

ity. The mass ratio of phospholipid to integral protein is nearly unity [10,11] and there is only one kind of protein, called rhodopsin (or opsin depending on the photochemical state), which is the photopigment, that accounts for 90–95% of its integral protein component [12–14]. Setting aside for the moment how these structural and chemical features bear upon the photoreceptor function of rod disks for scotopic vision [15], we note that the DMV constitutes a system of surprisingly simple structural entities that is amenable to a detailed probing of their electro-optical properties. This paper focuses on that point.

In our previous paper [16], we have shown that there exists a large field-induced birefringence for aqueous suspensions of DMV. The decay profile of the birefringence transient was found to be well represented by a single exponential function. We proposed to ascribe the birefringence transient to the rotatory orientation of the spherical vesicles, since the decay time constant is in accord with the rotatory relaxation time of a spherical shape with a radius of 450–480 nm.

In this paper, we shall start with the results of static measurements of the Kerr effect. This is divided into three parts. We will first show that there exists an enormous, negative electric anisotropy in a DMV which is deduced from the field dependence of the steady-state birefringence. Next, we present the determination of the specific Kerr constant and optical anisotropy from the concentration dependence of the Kerr constant and apparent saturation birefringence, respectively. Finally by combining the specific Kerr constant and optical anisotropy, we deduce another value of the electric anisotropy. Once these electro-optical characterizations are effected, we show how the osmotic deformation affects the optical anisotropy by an order of magnitude but not the electric polarizability anisotropy. We then propose a plausible birefringence mechanism model based on the known structural features of DMV and native disks in rod outer segments (ROS), and conclude by discussing how the model can account for the experimental results.

2. Experimental procedure

2.1. Materials

Bovine ROS disk membranes were isolated and purified from dark-adapted frozen retinae (American Stores Packing Company, Lincoln, Nebraska) by a modified version [5] of the method originally employed by Smith et al. [4]. The swollen membrane vesicles were suspended in 1 mM imidazole buffer with 50 μM EGTA. The suspension was filtered through a 2 μm pore size Nuclepore filter (Nuclepore Corp., Pleasanton, California) to remove dust and aggregated vesicles. The filter pore size was chosen to take into account the vesicle size of 1 μm diameter. In the previous work [16], we used 1 μm pore size filters although we did not specifically state it in the paper. The use of 1 μm filters gives rise to an absolute value of the birefringence nearly double that when a 2 μm filter is used. Thus, the 1 μm filter seems to give rise to some artifacts in the DMV preparations, possibly inducing fracture and resealing of the vesicles into smaller sizes. We have since confirmed that 2 μm is the lower limit of a safe filter pore size in this respect; a large pore size filter, e.g., 5 μm, does not further reduce the absolute value of the birefringence. In the study of medium osmolarity effect with sucrose, different concentrations of sucrose were added to the usual suspend-

ing medium (1 mM imidazole, 50 μM EGTA) in order to bring the final sucrose concentration of the medium to that reported. The concentration of the vesicles was determined by measuring the optical absorbance at 633 nm which provides a measure of the turbidity, since there is no absorption of membrane vesicles at 633 nm [17].

2.2. Kerr effect measurements

The apparatus for the Kerr effect measurements was as described in the previous work [16]. We used a quarter wave plate for linear detection of the birefringence. The output signal of a photomultiplier tube was recorded directly on a strip chart recorder as well as on a digital transient recorder (Biomation, model 802). The birefringence transient was monitored by a scope which displays the output of the transient recorder. We could monitor the steady-state birefringence expressed in the optical retardation, $\lim_{t\to\infty} \delta(t,E) \equiv \delta_0(E)$, as well as the transmitted light intensity by a strip chart recorder when the pulse duration was long (≈ 1 s) compared to the response time of the recorder. The electric field was applied in a sequence of bipolar rectangular pulses with the use of a pulse generator constructed in our laboratory. The pulse duration was varied with field strength from 1.5 s at 2 V/cm to 4 ms at 2.4 kV/cm, which was proven to be long enough to reach the steady-state birefringence. The pulse generator for low fields was designed to supply an electric pulse of 0.1–3.2 s duration with variable amplitude up to 40 V and with adjustable period of 1.3–37 s. It consists of a DC power supply and four optical switches operated by another pulse generator. In higher field experiments, above 40 V, another pulse generator was used as mentioned in the previous paper [16]. The Kerr cell and the experimental conditions are the same as those described in our previous report. The only difference was that bleached samples were used, since we had not found any significant difference between bleached and unbleached samples.

In the study of the sucrose osmolarity effect, the directions of the axes of the λ/4 plate and the analyzer were readjusted according to the optical rotatory power of the sucrose solution. Actually, the rotation due to the optical activity of a 20 mM sucrose solution amounts to no more than 1° at the end of a 20 cm Kerr cell. We have therefore ignored the correction to be made on the variable polarization axis within the cell relative to the field direction.

3. Results and discussion

3.1. Electric polarizability anisotropy

The electric field-induced birefringence, expressed as optical retardation in radians, reaches the steady-state value $\delta_0(E)$ within a pulse duration of 1.5 s for all cases reported here. In fig. 2 we show the dependence of $\delta_0(E)$ on the square of the field strength E^2 for three different number densities of DMV. The general profile of $\delta_0(E)$ versus E^2 appears to be independent of the DMV number density N when $\delta_0(E)$ is normalized by N provided it does not exceed 10^{10} vesicles/cm^3. A weak saturation behavior of the birefingence emerges at ≈ 60 V/cm although $\delta_0(E)$ does not completely level off. In order to examine the field strength range where $\delta_0(E)$ might level off, we have extended the field strength range up to 2.4 kV/cm. The steady-state birefringence $\delta_0(E)$ in fact does not level off but continues to rise with the field strength though with a much weaker

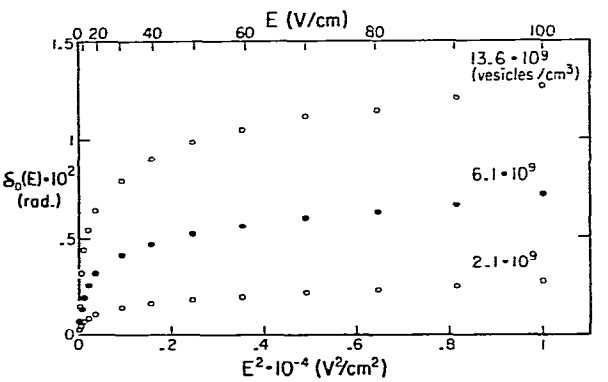

Fig. 2. Electric field dependence of the steady-state birefringence $\delta_0(E)$ for three different number densities of DMV.

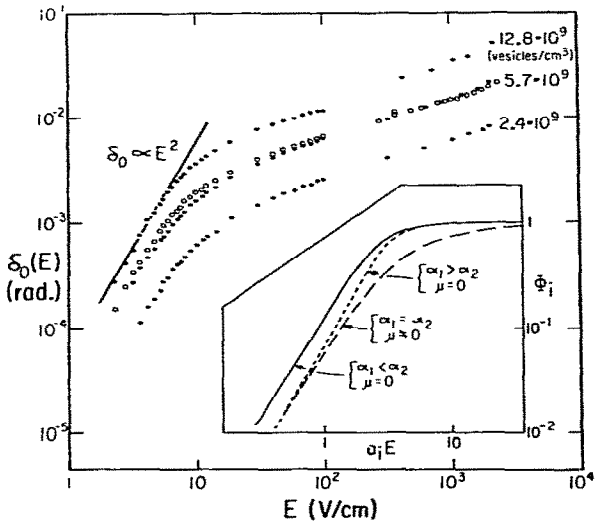

Fig. 3. Electric field dependence of the steady-state birefringence $\delta_0(E)$ in logarithmic scale for four different number densities of DMV. Theoretical curves in the inset show three limiting cases (see text for explanation).

dependence. In fig. 3, we show the behavior of $\delta_0(E)$ in the full range of fields examined, $2 \leqslant E \leqslant 2.4 \times 10^3$ V/cm. The data are for four samples of two independent DMV preparations. There is only a very limited field regime, below 6 V/cm, where the Kerr law, i.e., $\delta_0(E) \propto E^2$, is obeyed as indicated by the straight line.

In the inset, we show the three theoretical predictions for axially symmetric bodies developed by O'Konski et al. [18] and Shah [19];

$$\text{(I)}: \quad \alpha_1 = \alpha_2, \quad \mu \neq 0,$$
$$\text{(II)}: \quad \alpha_1 > \alpha_2, \quad \mu = 0,$$
$$\text{(III)}: \quad \alpha_1 < \alpha_2, \quad \mu = 0,$$

where α_1 and α_2 are the electric polarizability along the symmetry and transverse axes, respectively, and μ is the effective permanent dipole moment. The degree of orientation Φ_i ($i = $ I, II, III) represents a quantity equivalent to the normalized birefringence as

$$\Phi_i = \phi_i / \lim_{E \to \infty} \phi_i, \tag{1}$$

where

$$\phi_i = \int_0^{\pi} f_i(\theta) \tfrac{1}{2}(3\cos^2\theta - 1) 2\pi \sin\theta \, d\theta, \tag{2}$$

$$\lim_{E \to \infty} \phi_i = 1 \text{ for cases (I) and (II)},$$
$$= -\tfrac{1}{2} \text{ for case (III)}, \tag{3}$$

$f(\theta)$ is the orientational distribution function of the symmetry axis with respect to the external field direction at polar angle θ, and a_i ($i = $ I, II, III) are the shift factors of E defined as

$$a_{\mathrm{I}} = \mu/kT, \tag{4}$$
$$a_{\mathrm{II}}^2 = (\alpha_1 - \alpha_2)/kT, \tag{5}$$
$$a_{\mathrm{III}}^2 = (\alpha_2 - \alpha_1)/kT, \tag{6}$$

where kT has its usual meaning.

We shall defer the full discussion of these theoretical predictions until we reach fig. 4. It is sufficient here to note the following. The departure from the Kerr law behavior due to the saturation can be inferred for three different cases. The theoretical curves show that complete saturation due to the mechanism for low-field behavior must take place within the field range investigated if no high-field secondary mechanism exists. This, however, is not the case as shown in fig. 3. Thus, the high-field behavior appears to arise from a different mechanism than that responsible for the low-field behavior, hence we shall restrict our discussion to the latter, below 100 V/cm. The demarcation between the high- and low-field regimes is somewhat arbitrary, since there is no clear crossover point in the power-law regimes of $\delta_0(E)$ on E of the two.

Notwithstanding the ill-defined saturation behavior of $\delta_0(E)$ due to the secondary mechanism, we shall proceed with the analysis of data in the low-field regime, between 3 and 100 V/cm, with the use of the saturation theory. We show in fig. 4 all the data obtained at different number densities where $[\delta_0(E)/E^2]/[\delta_0(E)/E^2]_{E=0}$ is plotted against E^2 on a semi-logarithmic scale. An advantage of such a plot is to facilitate comparison with various theoretical predictions by laterally shifting the abscissa until the best match is obtained with the experimental saturation behavior.

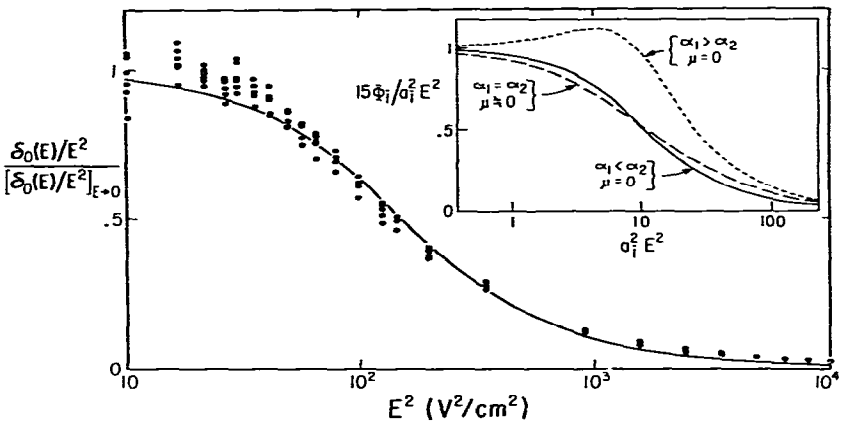

Fig. 4. $(\delta_0/E^2)/[(\delta_0/E^2)]_{E\to 0}$ versus log E^2. The best fit is obtained for the case of $\alpha_1<\alpha_2$, $\mu=0$ as shown by the solid curve. Other limiting cases are also shown in the inset for comparison.

Three specific limiting cases [20] stated above are considered for comparison with the data. In the inset, we again show the behavior of Φ_i for the three limiting cases in a different way by plotting $15\ \Phi_i/a_i^2E^2$ against $\log(a_i^2E^2)$. Setting aside for the moment whether the three chosen cases indeed include all possibilities, we see that case III gives rise to the best fit to the data as shown by the solid curve. In order to choose case III as the best match with experiment, we use the theoretical profiles in the intermediate region, $10^2 \leqslant E^2 < 10^3$ V^2/cm^2, as the most sensitive criterion because case I decays too gently, and case II decays too steeply in that region in addition to having a maximum.

Given the DMV structure as depicted in fig. 1, we can easily hypothesize that a DMV should not have any permanent dipole moment as long as the charge distribution due to photopigment molecules is uniform over either hemisphere. In that case, we need to consider only cases II and III. On the other hand, the saturation behavior and decay profile of case I shown in the insets of figs. 3 and 4, respectively, appear rather like those of case III, hence we have included it here for the sake of fair comparison. The elimination of case I as inferior to case III, purely on the basis of the fit to the data, is easily effected according to the above mentioned criterion, namely the $\delta_0(E)/E^2$ decay profile at $10^2 \leqslant E^2 \leqslant 10^3$ V^2/cm^2. Thus, we have grounds beyond physical argument to infer that there is no permanent dipole moment in DMV.

Finally, we obtain $\alpha_1 - \alpha_2 = -2.5 \times 10^{-10}$ cm^3 from the shift factor given in eq. (6) and the best-fit curve drawn in fig. 4. This is an enormously large value; we cite for comparison the corresponding quantity of tobacco mosaic virus (TMV) which is of the order of 10^{-14} cm^3 [18]. The four orders of magnitude difference may be ascribed to the entirely different kinds of induced dipole moment, i.e., the displacement of the photopigment for DMV (see below) and the ion atmosphere polarization for TMV [18].

In the next section, we will also show how the anisotropy $\alpha_1 - \alpha_2$ is determined by a totally different method and that its value agrees quite favorably with the present value.

3.2. *Specific Kerr constant and optical anisotropy*

Concentrating on the Kerr law regime of the electric field, we show in fig. 5 a plot of $\delta_0(E)$ versus E^2 on a linear scale at three different number densities of DMV. The slopes of the straight lines drawn give the Kerr constant according to the Kerr law;

$$\delta_0(E) = (2\pi Ln/\lambda_0)KE^2, \tag{7}$$

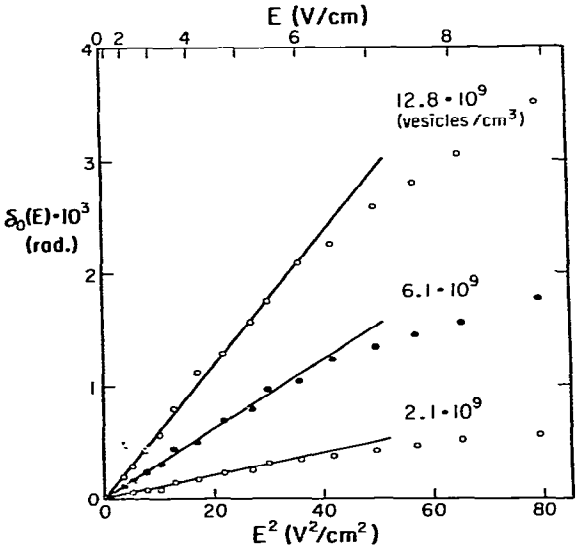

Fig. 5. Electric field dependence of the steady-state birefringence in the low-field regime. Straight lines show the Kerr law, i.e., $\delta_0(E) \propto E^2$.

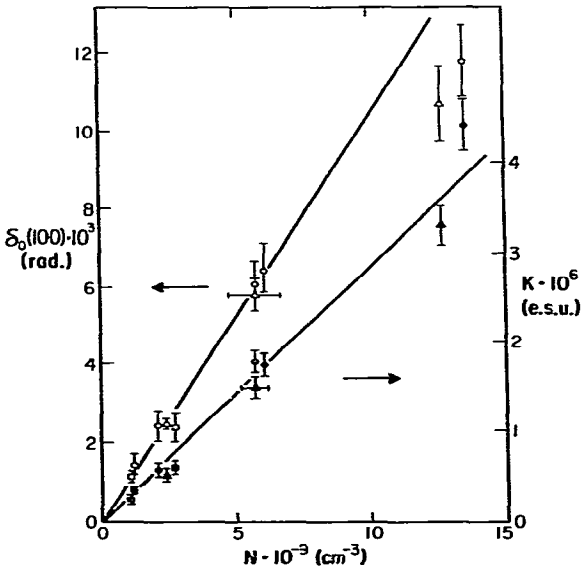

Fig. 6. Concentration dependence of the Kerr constant and of $\delta_0(100)$ as a measure of the saturation birefringence δ_s. The slopes yield respectively the specific Kerr constant and the optical anisotropy.

where K is the Kerr constant, L the cell length (12 cm), n the refractive index of the solution (1.333) and λ_0 the wavelength in vacuo (632.8 nm). The Kerr constant thus calculated is plotted against the number density N in fig. 6, whereby the slope of the linear plot is used to deduce the specific Kerr constant K_{sp} via

$$K = K_{sp} c_v = K_{sp} v N, \tag{8}$$

where c_v is the volume fraction of the DMV suspension and v is the volume of a DMV that is calculated by taking a vesicle radius of 0.46 μm as the best estimate from elastic light scattering. The value of K_{sp} so obtained is 7×10^{-4} statvolt^{-2} cm^2 in e.s.u. or 8×10^{-13} V^{-2} m^2 in SI units.

In fig. 6, we also plot $\delta_0(100)$ against N. As discussed in the previous section, we take $\delta_0(100)$ to be the apparent saturation limit of the birefringence δ_s for the primary mechanism. Though equating $\delta_0(100)$ with δ_s might be an overestimate, as is apparent from fig. 3, we can proceed to estimate the optical anisotropy $(g_1 - g_2)$ from the slope of such a plot via

$$\delta_s = \left[2\pi^2 L (g_2 - g_1)/n\lambda_0\right] c_v, \tag{9}$$

which applied to the case of a negative electric and optical anisotropy. We use eq. (9), since we have shown that $\alpha_1 - \alpha_2 < 0$ and that the sign of the birefringence is positive. The slope of the $\delta_0(100)$ versus N plot in fig. 6 yields $g_1 - g_2 = -1 \times 10^{-7}$. This is undoubtedly an overestimate, since we have used $\delta_0(100) = \delta_s$ because the saturation of the primary mechanism could easily have been reached at $E < 100$ V/cm.

We should emphasize here that K_{sp} determinations are infrequently effected by measurement of the concentration dependence of the Kerr constant K. In macromolecular systems, we know of only two instances, PBLG [21] and NaPES [22], where K_{sp} is so determined. More generally, K_{sp} is estimated from K at arbitrarily chosen E and c_v, since K_{sp} depends on concentration [23,24] and the Kerr law does not hold even for very weak field strengths. It is indeed noteworthy that the specific Kerr constant of 7×10^{-4} e.s.u. is remarkably large, and is quite comparable to that of TMV. To provide a better perspective on the magnitudes of

Table 1

Selected values of electric and optical anisotropy and specific Kerr constant of macromolecules and those of disk membrane vesicles in 1 mM imidazole

Materials	Solvent	M.W.	$\alpha_1 - \alpha_2$ (cm^3)	$g_1 - g_2$	K_{sp} (e.s.u.)	Ref.
TMV	distilled water	4.3×10^7	$(1-6) \times 10^{-14}$	6×10^{-3}	1.36×10^{-3}	[18]
PBLG	ethylene dichloride	3.5×10^5	8×10^{-16}	1.9×10^{-3}	1.3×10^{-5}	[21]
PBLG	ethylene dichloride	8.4×10^4	-	1.9×10^{-3}	2.3×10^{-6}	[21]
PBLG	dichloroethane/dimethylformamide	3.3×10^5	a)	4.3×10^{-1}	9×10^{-6}	[25]
PBLG	dichloroethane	1.95×10^5	a)	4×10^{-3}	3.3×10^{-6}	[18]
collagen	acetic acid	2.8×10^5	2.7×10^{-15}	1.7×10^{-3}	4.3×10^{-5}	[26]
NaPES	distilled water	2.4×10^4	a)	8×10^{-3}	1×10^{-5}	[18]
disk vesicle	1 mM imidazole	-	$-(1-3) \times 10^{-10}$	-1×10^{-7}	7×10^{-4}	present work

a) Not applicable because a permanent dipole moment is ascribed for the observed birefringence.

these quantities and a ready comparison, we collect in table 1 some representative values of $\alpha_1 - \alpha_2$, $g_1 - g_2$ and K_{sp}. Unlike the K_{sp} value, the optical anisotropy of a DMV was found to be very small compared to those of others in table 1. This also is entirely expected for DMV because of its nearly spherically symmetric body.

Now that we have on hand the specific Kerr constant and the optical anisotropy, it is possible to deduce the electric polarizability anisotropy with the use of these two quantities according to

$$\alpha_1 - \alpha_2 = (15n^2/2\pi)[kT/(g_1 - g_2)]K_{sp}. \quad (10)$$

This gives $\alpha_1 - \alpha_2 = -1.2 \times 10^{-10}$ cm^3 which is comparable to the value of -2.5×10^{-10} cm^3 obtained in the previous section. While the two differ by a factor slightly larger than 2, it is a remarkable agreement when we consider the disparate methods employed to deduce the two. The smaller (negative) value comes from the ratio $K_{sp}/(g_1 - g_2)$ which combines K_{sp} from the Kerr law regime with $g_1 - g_2$ from the saturation estimate of the primary mechanism, i.e., $\delta_s = \delta_0(100)$, hence it could easily be greater than the above estimate if the true value of δ_s were used to obtain $g_1 - g_2$. The larger (negative) value, on the other hand, is arrived at by comparing the experimental profile of the field dependence with the saturation theory for the entire field range supposed to be responsible for the primary mechanism, $3 \leq E \leq 100$ V/cm. Thus, a discrepancy by a factor of 2 is to be expected. We feel confident that the true value of $\alpha_1 - \alpha_2$ should lie in the range $-(1-3) \times 10^{-10}$ cm^3. This concludes our electro-optical characterization of DMV.

3.3. Osmotic deformation effect

As we have stated earlier that sucrose is an impermeable solute to DMV [7], it can thereby be used to raise the osmolarity of the suspending medium which will in turn cause DMV to undergo osmotic deswelling from the spherical to the oblate shell with its equatorial rim dimension intact [8]. We have performed two experiments designed to examine how such deformations affect the birefringence. We show sequentially the results of two

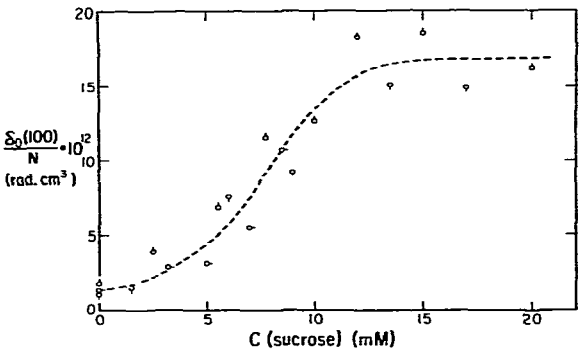

Fig. 7. Sucrose concentration dependence of $\delta_0(100)$ divided by the number density of DMV.

experiments and subsequently take up the discussion of their significance. The results of the first set of experiments are displayed in fig. 7 where the number density normalized apparent saturation birefringence $\delta_0(100)/N$ (at $E = 100$ V/cm) is plotted against sucrose concentration in suspending medium. A total of 19 samples from three independently prepared DMV are used and they are distinguished by different symbols. The dotted curve is drawn merely to aid the eye such that the overall trend of the osmotic deformation effect may be gleaned. The plot makes it quite clear that the birefringence increases dramatically, by an order of magnitude, with increasing concentration

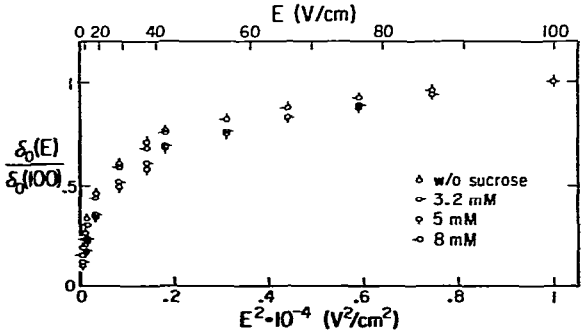

Fig. 8. Electric field dependence of the steady-state birefringence divided by $\delta_0(100)$ for four samples with different concentrations of sucrose.

of sucrose and this effect ceases at 13 mM sucrose. The second set of experiments examines the field dependent of birefringence at different extents of DMV osmotic deformation at $E \leq 100$ V/cm. The results are shown in fig. 8 where three sucrose concentrations in addition to the blank (without sucrose) are shown by different symbols. It is obvious that there exists no discernible difference in the field dependence of birefringence with sucrose concentration, at least up to 8 mM.

Turning to the significance of the first experiment, we can state unequivocally that the osmotic deformation of a DMV results in an increase in its birefringence by an order of magnitude and it reaches a well-defined saturation limit. This turns out to be quite consistent with another experiment recently concluded in this laboratory Extending the range of sucrose concentration beyond what had been examined earlier [8], Amis [27] has shown that the osmotic deformation of DMV by sucrose ceases at ≈ 12 mM and the shape of DMV has reached the disk shape limit at that concentration of sucrose. This must mean that the birefringence scales with the geometric eccentricity (axial ratio of oblate) of DMV and eventually attains the limiting value when DMV can no longer deform beyond the disk shape. Thus, the entire profile displayed in fig. 7 represents the effect of geometric eccentricity of DMV from the spherical shell to the disk shape which may correspond to that of the native disks in the retinal rods. The results collected in fig. 8, on the other hand, demonstrate that there is hardly any change in the electric anisotropy with the eccentricity, at least up to 8 mM sucrose because the field dependence is seen to be alike for all sucrose concentrations. Combining these two findings, we finally reach the conclusion that the geometric eccentricity of DMV affects only the optical anisotropy while it scarcely influences the electrical anisotropy. A negative sign of the optical anisotropy is to be expected, since a flat disk must have a negative sign as Shah has shown for a disk-shaped clay, bentonite [19]. Since the birefringence is positive, this should result in a negative electric anisotropy.

3.4. Quadrupolar field effect

A Kerr cell with its electrode configuration modified for use in a quadrupolar field was constructed. The electrode configuration is depicted in fig. 9, which shows a cross-sectional view of the cell. The electric field is applied in such a way that the pair of platinum wires is at the opposite electric pole relative to the pair of Pt plates. Nitrobenzene was used as a test liquid to check the working of the quadrupolar electrodes which were found to be satisfactory. Upon application of different quadrupolar fields, a birefringence of equal or slightly smaller magnitude was detected at the same applied potential as in the case of a dipolar field.

With DMV suspensions in the Kerr cell, however, we were *not* able to observe any birefringence signal in the quadrupolar mode. A given suspension which gives rise to a steady-state birefringence of 10^{-3} rad at ≈ 5 V/cm in the dipolar mode (either across the plates or the wires) does not produce any detectable birefringence signal in the quadrupolar mode. This observation will be invoked as supporting evidence for the birefringence model presented below.

3.5. Model of the birefringence mechanism

Before we come to proposing a model for the birefringence mechanism of DMV, it might be helpful to review the structural features of DMV based on light-scattering results [5,8] and other

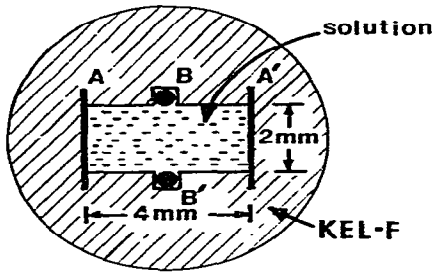

Fig. 9. Electrode configuration for the application of a quadrupolar field: electrodes A, A' are at one potential and B, B' at the other potential in the quadrupolar mode.

morphological studies of the native disks in ROS. From the osmotic deswelling experiment of fully swollen, spherical shell-shaped DMV [5], it was found that a DMV deforms into an oblate shell with its semi-major axis unchanged [8]. Thus, it was concluded that there must be a structural feature within a DMV that resists the osmotic deformation, hence is different from the rest of the membrane constitution. We call this the equatorial rim as shown in fig. 1. Furthermore, we think it quite probable that the equatorial rim in a DMV is the same structure that Sjoestrand and Kreman [9] find around the disk edge of ≈ 0.2 μm in width which is thicker than the rest of the disk and contains particles on the cytoplasmic surface in the native disks of ROS. Complementary to this finding is the observation by Papermaster et al. [28] that a large protein with molecular weight of 290000 dalton is localized around the disk edge in native ROS. Thus, from these three separate observations, the rim may be characterized as a structurally distinct entity dividing at the equator the two hemispheres within a DMV. We therefore attribute the source of the optical polarizability anisotropy to the rim; that is, it is slightly more polarizable along an axis within the rim plane (transverse axis) than along the symmetry axis normal to the rim plane by virtue of the observed small and negative anisotropy, i.e., $g_1 - g_2 \lesssim 0$. From the known phospholipid topology and composition of disk membranes [29] and the partial amino acid sequencing of the photopigment, rhodopsin [30], it is entirely reasonable to assume that some of the polar heads of phospholipids and photopigment molecules are anionically charged at pH 7 with ionic strength in the mM range. In addition, the electrophoretic mobility of a DMV under such conditions is used to assign $\approx 10^4$ as the electrokinetically active electronic charges per DMV [31]. Further, it is well established that photopigment molecules undergo lateral diffusion on the disk surface with a coefficient of $\approx 10^{-9}$ cm^2/s [32–34].

We therefore postulate that photopigment molecules execute field-induced displacements within each hemisphere of a DMV but cannot cross the equatorial rim because it acts as a displacement barrier; hence the rim separates one hemisphere from the other as the displacement domain of a given photopigment molecule. By a field-induced displacement, we mean a very slight perturbation from the unperturbed uniform distribution of photopigments whose mean nearest-neighbor distance is estimated to be ≈ 33 Å and there are $\approx 8 \times 10^4$ photopigments per DMV [17]. Prior to application of an external electric field, there exists a uniform distribution of photopigments on both hemispheres and a random orientation of the rim plane relative to the laboratory axes. With the field on, the photopigment distribution is perturbed from the uniform one, resulting in excess negative charges around the equatorial rim toward the positive electrode. This gives rise to a slowly induced dipole moment in the equatorial plane which is not yet aligned with the field. The dipole moment so induced in turn exerts torque on a DMV so as to orient its rim plane parallel to the applied field direction. Thus, the rim plane alignment with its preferential optic axis results in the observed birefringence. When the field is off, the photopigment distribution returns to the unperturbed one whereby the slowly induced dipole moment is gradually lost and the rim plane alignment returns to the random orientation. Thus, the recovery process manifests itself in the global reorientation of a whole DMV with a time constant characteristic of the rotatory diffusion of a sphere with radius of 450–480 nm. This we have demonstrated to be the case [16]. Our proposed mechanism thus contains several ingredients, some of which will be addressed below. We do not, however, purport to have proven the validity of the model. We claim only to have sought its plausibility.

Our model first of all can account for the observed large and negative electric polarizability anisotropy. The model calls for the 'accumulation' of negatively charged photopigments around the rim at one pole of DMV and the 'depletion' at the other pole when the field is applied. Hence, the electric polarizability is greater along the transverse axis, lying in the rim plane, than along the symmetry axis. The large magnitude of the anisotropy, $\approx 10^{-10}$ cm^3 compared to $\approx 10^{-14}$ cm^3 of tobacco mosaic virus, can also be explained easily if one takes into account the size of DMV. Sup-

pose the charge imbalance on the DMV surface at the steady state with the field on is one unit (electronic) charge at each pole, then the DMV would have an apparent induced dipole moment of 4.8×10^4 debye due to its diameter of 1 μm. In other words, the sheer size of DMV coupled with the total numer of photopigments per DMV can well explain the magnitude of the electric anisotropy without invoking substantial perturbation of the uniform photopigment distribution at the field-free state. Thus, our model discounts any contribution from field-induced optical anisotropy to the total steady-state birefringence. This should be true only in the low-field regime to which our model is restricted. Direct support of this contention is provided by the negative observation in the quadrupolar field. If there were any field-induced optical anisotropy contributing to the birefringence, we should have detected the signal in the quadrupolar mode because photopigment displacement should occur in this field configuration as easily as in the dipolar mode. The absence of the birefringence signal is due to lack of alignment of the rim plane relative to the laboratory axes because contrary to the dipolar mode there exists no torque acting on DMV to orient its rim plane in the quadrupolar mode. Hence, the intrinsic optical anisotropy afforded by the rim structure and its alignment with respect to the laboratory axes alone are responsible for the observed birefringence.

We now come to the osmotic deswelling experiment with sucrose. That the optical anisotropy depends strongly on the geometric eccentricity, i.e., the axial ratio of the oblate shell, does not require further justification, for it must reach the limiting negative value at the disk-shaped state much like that of the bentonite particle as Shah has shown [19]. The increase by an order of magnitude of $g_1 - g_2$ is not unreasonable when we consider the DMV shape to change from a spherical shell to disk shape with its semi-major axis conserved. The relative constancy of the electric polarizability anisotropy with respect to the geometric eccentricity, however, requires some explanation in terms of our model. Note that the surface area decrease from the spherical shell to the disk limit amounts to a factor of two, i.e., $4\pi r^2$ to $2\pi r^2$. Since the photopigment number on each hemisphere of a DMV must be conserved throughout the osmotic deswelling, the field-induced displacement at the same field strength should moderate as the surface area of DMV decreases with increasing axial ratio because the surface area per photopigment at ≈ 40 nm^2 [17] decreases by a factor of two. The projection onto the rim plane of the net displacement on each hemisphere amounts to a measure of the electric polarizability along the transverse axis. While the net displacement decreases with increasing axial ratio of the DMV, its projection onto the rim plane could remain relatively the same, resulting in the constancy of the electric anisotropy as DMV deswelling proceeds from the spherical shell to the disk shape limit. Again, we present this argument as plausible but not without equivocation.

The foregoing are presented to provide some credence to our proposed model. However, we recognize that a good deal of testing must be done before the model is said to be proven. We must parenthetically remark that we have ignored the contribution of counterions either to the orientation mechanism or to the resulting birefringence. Whether that is justified remains to be tested by varying ionic strengths. More important is a crucial testing of the model relative to the photopigment displacement in terms of the dynamic Kerr effects. We have recently reported such a study [35]. At the risk of repetition we reiterate that our model is applicable in the relatively weak electric field region, possibly below 100 V/cm. When the field exceeds this limit, it is quite possible that another mechanism would be elicited such as dielectric deformation of the DMV away from its spherical shell shape, similar to that which O'Konski has proposed for artificial phospholipid vesicles [36]. In the high-field regime, we have in fact observed several faster components in the birefringence decay profile other than the global orientation mechanism [16]. Such a high-field-induced mechanism by itself is also an interesting problem which may be related to the high-field pulse-induced changes in the membrane permeability [37].

Acknowledgement

This work is supported in part by NIH grant EY01483 and by an NIH Biochemical Sciences Support Grant administered through the Graduate School of the University of Wisconsin, Madison. We acknowledge the assistance of T.J. Weight and D.K. Bilich in the design and construction of the pulse generator.

References

[1] F. Jähnig, Biophys. Chem. 4 (1976) 309.
[2] H. Träuble, M. Teubner, P. Woolley and H. Eibl, Biophys. Chem. 4 (1976) 319.
[3] R.C. Crain, G.V. Marinetti and D.F. O'Brien, Biochemistry 17 (1978) 4186.
[4] H.G. Smith Jr., G.W. Stubbs and B.J. Litman, Exp. Eye Res. 20 (1975) 211.
[5] T. Norisuye, W.F. Hoffman and H. Yu, Biochemistry 15 (1976) 5678.
[6] M.J. Yeager, in: Neutron scattering for the analysis of biological structures, ed. B.P. Schoenborn (National Technical Information Service, Springfield, VA, 1976) p. III–1.
[7] A. Darszon, M. Montal and J. Zarco, Biochem. Biophys. Res. Commun. 76 (1977) 820.
[8] T. Norisuye and H. Yu, Biochim. Biophys. Acta 471 (1977) 436.
[9] F.S. Sjoestrand and M. Kreman, J. Ultrastruct. Res. 65 (1978) 195.
[10] F.J.M. Daemen, W.J. DeGrip and P.A.A. Jansen, Biochim. Biophys. Acta 271 (1972) 419.
[11] F.J.M. Daemen, Biochim. Biophys. Acta 300 (1973) 255.
[12] W.E. Robinson, A. Gordon-Walker and D. Bownds, Nature, New Biol. 235 (1972) 112.
[13] J.K. Blasie, C.R. Worthington and M.M. Dewey, J. Mol. Biol. 39 (1969) 407.
[14] W. Krebs and H. Kühn, Exp. Eye Res. 25 (1977) 511.
[15] G. Wald, Science 162 (1968) 230.
[16] H. Takezoe and H. Yu, Biophys. Chem. 13 (1981) 49.
[17] E.J. Amis, D.A. Davenport and H. Yu, Anal. Biochem. 114 (1981) 85.
[18] C.T. O'Konski, K. Yoshioka and W.H. Orttung, J. Phys. Chem. 63 (1959) 1558.
[19] M.J. Shah, J. Phys. Chem. 67 (1963) 2215.
[20] E. Fredericq and C. Houssier, Electric dichrosim and electric birefringence (Clarendon Press, Oxford, 1973) p. 27.
[21] I. Tinoco Jr., J. Am. Chem. Soc. 79 (1957) 4336.
[22] K. Yoshioka and C.T. O'Konski, J. Polymer Sci. A 2 6 (1968) 421.
[23] H. Nakayama and K. Yoshioka, J. Polymer Sci. A3 (1965) 813.
[24] J.C. Powers Jr. and W.L. Peticolas, Biopolymers 9 (1970) 195.
25] K. Nishinari and K. Yoshioka, Kolloid-Z. A. Polymere 240 (1970) 831.
[26] K. Yoshioka and C.T. O'Konski, Biopolymers 4 (1966) 499.
[27] E.J. Amis, Ph.D. Thesis, University of Wisconsin (Madison, Wisconsin, 1981).
[28] D. Papermaster, B.G. Schneider, M.A. Zorn and J.P. Kraehenbuhl, J. Cell Biol. 78 (1978) 415.
[29] R.C. Crain, G.V. Marinetti and D.F. O'Brien, Biochemistry 17 (1978) 4186.
[30] P.A. Hargrave, S.-L. Fong, J.H. McDowell, M.T. Mass, D.R. Curtis, J.K. Wang, E. Juszczak and D.P. Smith, Neurochem. Int. 1 (1980) 231.
[31] G.B. Caflisch, Ph.D. Thesis (University of Wisconsin, Madison, Wisconsin, 1979); G.B. Caflisch and H. Yu, to be published.
[32] M. Edidin, Annu. Rev. Biophys. Bioeng. 3 (1974) 179.
[33] M. Poo and R.A. Cone, Nature 247 (1974) 438.
[34] P.A. Liebman and G. Entine, Science 185 (1974) 457.
[35] H. Takezoe and H. Yu, Biochemistry 20 (1981) 5275.
[36] C.T. O'Konski, in: Transport in proteins, eds. G. Blauer and H. Sund (de Gruyter, New York, 1979) p. 231.
[37] K. Kinosita Jr. and T.Y. Tsong, Nature 272 (1978) 258.